PHYSICAL REVIEW B VOLUME 27, NUMBER 6 15 MARCH 1983

Structural phase stability in third-period simple metals

A. K. McMahan and John A. Moriarty
Lawrence Livermore National Laboratory, University of California, Livermore, California 94550
(Received 29 November 1982)

Extensive phase-stability calculations for the fcc, hcp, and bcc structures of Na, Mg, Al, and Si are reported both near 1 atm and under high pressure, where Si becomes a natural member of this set of third-period simple metals. Calculations for each element have been carried out by two entirely different first-principles techniques: the generalized pseudopotential theory (GPT) and the linear-muffin-tin orbitals (LMTO) method. The two techniques give results in good qualitative agreement for Mg, Al, and Si, and predict sequences of high-pressure structural phase transitions for these elements which arise from the lowering and partial filling of the initially empty $3d$ band under compression. Detailed analysis shows that major trends in the phase stability of the third-period metals are correlated with specific features both in the LMTO one-electron densities of states and in the GPT interatomic pair potentials. Quantitative comparisons between the two theoretical techniques, as well as with available experimental data and other recent calculations, are further used to assess the accuracy of the approximations employed by these methods in calculating structural energy differences.

I. INTRODUCTION

The study of crystal-phase stability in solids has progressed dramatically over the last few years. Experimentally, advances in diamond-anvil technology[1] have extended the accessible pressure range at room temperature to nearly 100 GPa (1000 kbar) and have led to a wealth of newly discovered high-pressure structural phase transitions.[1,2] At the same time, theoretical studies have shown that rigorous implementations of the Kohn-Sham local-density-functional formalism,[3] through such widely varying first-principles techniques as the *ab initio* pseudopotential (AP) method,[4,5] generalized pseudopotential theory (GPT),[6,7] and the linear muffin-tin orbitals (LMTO) method,[8–10] yield phase stability predictions in generally good qualitative agreement with each other and with experiment. This is a significant accomplishment given the exceedingly small energy differences between phases that must be calculated, often 2 or more orders of magnitude smaller than the cohesive energy.

Recent theoretical calculations have shed light on many of the trends in crystal structure apparent throughout the Periodic Table, both near normal density and under high pressure. Of particular interest has been the discovery that d electrons play a critical role in determining the stable structures of not only the transition metals but also of the lanthanide, alkaline-earth, and group-IIB metals as well. Trends which seem to be so explained include the hcp→bcc→hcp→fcc sequence of structures from left to right across the transition metals,[9,11] and the hcp→Sm-type→dhcp→fcc sequence for the lanthanides both with decreasing atomic number and under pressure.[12,13] The lanthanide sequence of transitions has also been observed[14] in compressed Y, corroborating the belief that f electrons are not involved in determining this sequence. In the case of the alkaline-earth metals, trends explained by the presence of d electrons include the hcp→fcc→bcc sequence observed with increasing atomic number,[15,16] the fcc→bcc→hcp sequence observed[17] for the heavier members under pressure,[16] and the temperature-induced fcc→bcc transitions in Ca and Sr.[15] Finally, the high c/a axial ratios found in the hcp group-IIB metals Zn and Cd have also been attributed to the effects of d electrons.[6,7]

In a preliminary account of the present work,[18] we reported on a series of GPT and LMTO phase-stability calculations for the metals Na, Mg, and Al over a wide range of volume. We demonstrated that under compression the controlling influence of d electrons is extended to even such simple metals, leading to newly predicted sequences of high-pressure structural phase transitions in each case. Earlier phase-stability calculations for Al by Friedli and Ashcroft[19] were not carried to sufficiently high compression to detect these transitions. Our predictions for Al, however, have recently been theoreti-

cally confirmed by the AP calculations of Lam and Cohen.[20] In this paper, we present a more detailed description of our work on these third-period simple metals, as well as extensive new results and analyses. To better account for the effects of the d electrons in the GPT, we have here applied the more appropriate empty-d-band limit of that theory in place of the simple-metal limit used previously. This leads to generally better agreement with both LMTO and AP results at high pressure. We include new LMTO calculations for Na and a description of our tests of the LMTO force-relation technique for calculating structural energy differences, which was omitted in the earlier work. We have also included new high-pressure results for Si, which becomes a natural member of this set of third-period simple metals under compression.

In the remainder of the paper, the GPT and LMTO computational techniques are briefly described in Sec. II and our calculated results on phase stability are presented in Sec. III. In Sec. IV we focus on the qualitative trends predicted and try to gain some insight into the mechanisms determining phase stability in the third-period elements by examination of the LMTO one-electron densities of states and the GPT interatomic pair potentials. Critical quantitative comparisons between the predictions of the two theoretical methods, as well as with experiment and recent AP calculations, are given in Sec. V, and our conclusions are given in Sec. VI.

II. CALCULATIONAL TECHNIQUES

Our analysis of phase stability in the third-period simple metals is confined to zero temperature and is based on calculations of the total energy of each solid as a function of atomic volume Ω and crystal structure (fcc, ideal hcp, and bcc lattices). We have found the total-energy differences between structures at fixed volume $\Delta E_{\rm tot}$ to be almost identical to the Gibbs free-energy differences at fixed pressure ΔG, and so we focus only on the former. This simplification is a direct consequence of the fact that at a given pressure, the atomic volumes amongst the metallic structures we consider differ only slightly (typically, $\Delta\Omega/\Omega$ is less than 0.01). As shown in Ref. 15, the leading correction to $\Delta G=\Delta E_{\rm tot}$ for two structures differing in volume by $\Delta\Omega$ is $\frac{1}{2}\Omega B(\Delta\Omega/\Omega)^2$, where B is the bulk modulus. In the present work, this term is generally about 2 orders of magnitude smaller than $\Delta E_{\rm tot}$.

We calculate the total energy (excluding zero-point vibrational corrections) within the general framework of the Kohn-Sham local-density formalism[3] by means of both the GPT and LMTO methods. Zero-point energies have been obtained separately with the GPT method, but, except in Na near normal conditions, they are of negligible importance and are not included in our results unless specifically noted. As applied here, the GPT and LMTO methods employ slightly different forms for the exchange-correlation potential in the Kohn-Sham equations. The GPT uses a modified Hedin-Lundqvist form appropriate for the unique requirements of that theory,[6,21] while the present LMTO calculations are based on the closely related exchange-correlation potential of von Barth and Hedin.[22] Test calculations have shown, however, that this difference is not significant relative to other differences in the two methods.

A. GPT method

The density-functional formulation of the GPT is discussed at length in Refs. 6 and 7. In the present work we utilize the latter optimized version of the theory. For a d-band metal the essence of the method is to work in an enlarged basis set consisting of both plane waves $|\vec{k}\rangle$ and localized d states ϕ_d, and analytically develop the electron density and total energy in suitable expansions involving small quantities. The ultimate expansion parameters are the following: a pseudopotential w_0 and a d-state hybridization potential $\Delta_{\rm vol}$. The state of the art is to calculate the electron density to first order in w_0 and $(\Delta_{\rm vol})^2$ and the total energy to second order in these quantities. This provides internal self-consistency while retaining the dominant structural contribution to the total energy $E_{\rm tot}$. Moreover, in such a development the small structural energy $E_{\rm struc}$ is isolated from the much larger volume contribution $E_{\rm vol}$,

$$E_{\rm tot}=E_{\rm vol}+E_{\rm struc}\ . \tag{1}$$

Thus in obtaining the total-energy difference between two lattices at fixed volume only $E_{\rm struc}$ enters the calculation and a meaningful result can be obtained no matter how small the energy difference. For a perfectly periodic lattice $E_{\rm struc}$ can be calculated from the simple expression

$$E_{\rm struc}=\tfrac{1}{2}(Z^*e)^2\left[\frac{1.8-\alpha_E}{S}-\sum_{\vec{G}}{}'\frac{4\pi}{\Omega G^2}F_N(G)\right], \tag{2}$$

where Z^* is the effective valence of the metal, α_E is the electrostatic Ewald (or Madelung) constant of the lattice ($\alpha_E=1.791\,75$ for fcc, 1.791 68 for ideal hcp, and 1.791 86 for bcc), S is the Wigner-Seitz radius ($\Omega=4\pi S^3/3$), and F_N is the so-called normalized energy-wave-number characteristic. The second

term in Eq. (2) is the band-structure energy and the sum is over all nonzero reciprocal-lattice vectors $\vec{G}$. The quantities Z^* and F_N are volume-dependent but structure-independent functions of w_0 and $\Delta_{\rm vol}$ which characterize the metal for an arbitrary arrangement of the ions at fixed volume and can be used to calculate essentially all structural properties related to the total energy including phonons.

In the GPT there are several natural limits or forms of the theory depending on the nature and filling of the d bands. For the third-period simple metals up to about fivefold compression, the two of interest are the so-called simple-metal limit and the empty-d-band limit. In the former, all d states are implicitly treated as free-electron-like and in that regard are not distinguished from s and p states. This situation well characterizes Na, Mg, and Al under normal conditions ($\Omega/\Omega_0=1.0$). As we found in our preliminary work, however, the initially empty $3d$ band above the Fermi level lowers, narrows, and eventually hybridizes with the valence s and p states below under compression. This hybridization effect is missed in the simple-metal limit but is explicitly taken into account in the empty-d-band limit. In either case, however, the net effect of the d states is embodied in the characteristic functions Z^* and F_N. The empty-d-band F_N turns out to be expressible in the same mathematical form as the simple-metal result with a modified Z^* and an effective pseudopotential

$$\langle \vec{k}+\vec{q}\,|\,w\,|\,\vec{k}\rangle=\langle \vec{k}+\vec{q}\,|\,w_0\,|\,\vec{k}\rangle+\sum_d \frac{\langle \vec{k}+\vec{q}\,|\,\Delta_{\rm vol}\,|\,\phi_d\rangle\langle\phi_d\,|\,\Delta_{\rm vol}\,|\,\vec{k}\rangle}{(\epsilon_{\vec{k}}-E_d^{\rm vol})}\ , \tag{3}$$

where

$$\langle \vec{k}+\vec{q}\,|\,w_0\,|\,\vec{k}\rangle=v(q)+\sum_{\alpha=c,d}(\epsilon_{\vec{k}}-E_\alpha^{\rm vol})\langle \vec{k}+\vec{q}\,|\,\phi_\alpha\rangle\langle\phi_\alpha\,|\,\vec{k}\rangle + \sum_d(\langle \vec{k}+\vec{q}\,|\,\Delta_{\rm vol}\,|\,\phi_d\rangle\langle\phi_d\,|\,\vec{k}\rangle+\text{c.c.})\ . \tag{4}$$

In Eqs. (3) and (4), v is the full (single-site) self-consistent potential, $\epsilon_{\vec{k}}=\hbar^2k^2/2m$, and $E_c^{\rm vol}$ and $E_d^{\rm vol}$ are the (volume-dependent) energies of the inner-core states ϕ_c and d states ϕ_d, respectively. Equation (3) represents an optimized choice of pseudopotential with the zero of energy in $E_c^{\rm vol}$ and $E_d^{\rm vol}$ taken at the bottom of the valence band. The d-basis states ϕ_d used in the present work were constructed according to the universal prescription adopted in Ref. 7.

Other quantities of interest here may also be obtained within the general framework of the GPT. Pressure, for instance, can be calculated by direct numerical differentiation of $E_{\rm tot}(\Omega)$. Elements of the band structure, useful for comparison with the LMTO method, may be simply related to matrix elements of w_0 and $\Delta_{\rm vol}$. In this regard, two of the most revealing states are the X_1 and X_4' levels in the fcc structure. The former is a d-hybridized state and in a two-plane-wave approximation is given (relative to the bottom of the valence band) by

$$\epsilon(X_1)=\tfrac{1}{2}\{(A+E_d^{\rm vol})-[(A-E_d^{\rm vol})^2+8B]^{1/2}\}\ , \tag{5}$$

where

$$A=\epsilon_{\vec{k}_0}+\langle \vec{k}_0\,|\,w_0\,|\,\vec{k}_0\rangle+\langle -\vec{k}_0\,|\,w_0\,|\,\vec{k}_0\rangle$$

and

$$B=\sum_d\langle -\vec{k}_0\,|\,\Delta_{\rm vol}\,|\,\phi_d\rangle\langle\phi_d\,|\,\Delta_{\rm vol}\,|\,\vec{k}_0\rangle\ ,$$

with $k_0=2\pi/a$. The unhybridized X_4' level, on the other hand, is pure p-like and is given to the same approximation by

$$\epsilon(X_4')=\epsilon_{\vec{k}_0}+\langle \vec{k}_0\,|\,w_0\,|\,\vec{k}_0\rangle-\langle -\vec{k}_0\,|\,w_0\,|\,\vec{k}_0\rangle\ . \tag{6}$$

Finally, phonon spectra and zero-point vibrational energies $E_{\rm ph}$ can be calculated from Z^* and F_N by standard procedures. This has been done in the present work for the fcc and bcc lattices at each volume considered. In addition, whether or not imaginary phonon frequencies are obtained provides useful information on the mechanical stability of these lattices. Corresponding information on the mechanical stability of the ideal hcp structure has been obtained by calculating $E_{\rm struc}$ as a function of the c/a axial ratio between 1.5 and 2.0 in each case.

B. LMTO method

The LMTO method has also been described in detail elsewhere.[8,9,23] In the present calculations, as previously,[10,18] we have employed the atomic-sphere approximation,[8] according to which each Wigner-Seitz polyhedron is approximated by a sphere in which the electron density is spherically averaged.

All electrons have been treated self-consistently and all but the 1*s* electrons have been treated in a band mode. The 3*s*, 3*p*, and higher-lying states were generally sampled with 505, 252, and 506 points in the irreducible wedges of the fcc, hcp, and bcc Brillouin zones, respectively, while coarse sampling was used for the filled narrow 2*s* and 2*p* bands. These choices insure convergence of the total energy to better than 0.1 mRy per atom, which is the dominant numerical uncertainty in our LMTO calculations. Except as indicated otherwise, calculations were carried out including *s*, *p*, and *d* components in the angular-momentum basis. Test calculations including *f* components showed only slight changes in the structural energy differences at the highest compressions considered. All LMTO calculations reported in this paper include the combined-correction term to the atomic-sphere approximation used in the LMTO method.[8]

The total energy (per atom) has been evaluated by the expression

$$E_{\rm tot}=\frac{1}{N}\sum_i \epsilon_i - 2\pi\int_0^S dr\, r^2\rho(r)\left[\frac{Ze^2}{r}+V(r)+v_{\rm xc}(r)-2\epsilon_{\rm xc}(r)\right], \tag{7}$$

where ϵ_i are the one-electron eigenvalues, $\rho(r)$ is the spherically averaged electron density, $V(r)$ is the total one-electron potential, and $v_{\rm xc}(r)$ and $\epsilon_{\rm xc}(r)$ are the exchange-correlation potential and energy density, respectively. The index i is intended to run only over occupied states and includes core as well as valence levels. Equation (7) may be viewed as arising from the usual muffin-tin expression[24] for the total energy in the limit that the muffin-tin radius is extended to the Wigner-Seitz radius. In this approach, however, one obtains an additional term which has been variously called the muffin-tin[25] or Ewald[26] correction to the total energy in the LMTO method,

$$\tfrac{1}{2}[\rho(S)\Omega e]^2\frac{1.8-\alpha_E}{S}\ . \tag{8}$$

Although this correction is clearly the analog of the electrostatic contribution to the GPT structural energy in Eq. (2), it differs importantly from the latter in that $\rho(S)\Omega$ is structure dependent while Z^* is not. We have *not* included the correction Eq. (8) in our LMTO structural-energy-difference calculations as it worsens LMTO agreement with the present GPT results as well as with AP calculations for Si.[10] While this may seem inconsistent, it is to be noted that Eq. (2) appears in a rigorous perturbation expansion while Eq. (8) is derived from a muffin-tin approximation which itself needs further electrostatic correction. It is probably not the form of Eq. (8), but most likely the appearance of the effective charge as $\rho(S)\Omega e$ which is suspect and causes more harm than good when Eq. (8) is used in LMTO structural-energy-difference calculations. To put the matter in perspective, however, only at the largest volumes we consider does Eq. (8) affect the LMTO calculated structural energy differences by as much as 25%.

Pressure has been evaluated using the Pettifor-Liberman surface integral expression.[27] The muffin-tin or Ewald correction affects the calculated pressures by more than 5% only for Al and Si in the few Mbar range and below. We have included this correction in our pressure calculations, however, since our experience has been that it generally yields improved agreement with experiment in the case of the pressure-volume curve. Also in this regard, our LMTO-calculated pressures appear to be more accurate than those derived from the GPT method due to the neglect of third- and higher-order total-energy terms in the latter. For this reason, and also to establish a universal scale for converting volume to pressure, we have used LMTO pressures in our analysis below, except as noted.

C. LMTO force-relation technique

Calculation of structural energy differences using Eq. (7) requires a separate self-consistent calculation of the total energy for each lattice being investigated. One must then subtract these huge all-electron total energies to get the small energy differences between phases. The force-relation technique[28] offers an elegant way of circumventing both the need for performing multiple self-consistent calculations as well as that of subtracting very large and nearly equal numbers. It is based on the result, rigorous within the local-density approximation, that the net change in total energy caused by a distortion of the lattice is given to first order by

$$\delta E_{\rm tot}=\frac{1}{N}\delta\sum_i \epsilon_i+\delta E_M\ . \tag{9}$$

The change in one-electron eigenvalues ϵ_i and in the electrostatic Madelung energy E_M is to be computed by a restricted variation δ in which the total one-electron potential is rigidly shifted but not otherwise changed by the lattice distortion.[28]

The meaning of the restricted variation is particularly simple for the LMTO method. As dictated by

the atomic-sphere approximation,[8] all lattices are treated by a neutral Wigner-Seitz sphere within which the one-electron potential is defined. One thus uses the *same* potential to calculate several sets of eigenvalues according to different boundary conditions at the sphere surface appropriate to the various lattices under consideration. Only one self-consistent calculation is required (to get the potential), and only the valence eigenvalues enter the sum in Eq. (9), provided the core eigenvalues are unaffected by changes in boundary conditions at the sphere surface. (In the present work, changes in the $2s$ and $2p$ energy levels are small but not negligible, and they should be included at least for Na and Mg.) Furthermore, $\delta E_M \equiv 0$ within the atomic-sphere approximation since the electrostatic Madelung energy is approximated by that of the neutral Wigner-Seitz sphere ($\alpha_E = 1.8$), which is unaffected by the change in structure.

The essential question posed by the use of Eq. (9), as, for example, in Refs. 9, 11, 13, and 16, is whether or not a change in structure from, say, fcc to bcc, qualifies as a "first-order" distortion of the lattice. We have carried out extensive tests of this question for the fcc, hcp, and bcc phases of Na, Mg, Al, and Si over the full range of atomic volumes considered in this work. We have generally found the structural energy differences calculated from Eqs. (7) and (9) to agree within 2%, or for the smaller differences, to within 0.05 mRy/atom. It is apparent, therefore, that changes from one to another of the fcc, hcp, and bcc structures *do indeed qualify as first order* in the sense required by Eq. (9). In these cases the force-relation technique offers an excellent approximation to the correct structural energy differences obtained by fully self-consistent calculation of the total energy for each lattice. While the principal LMTO results reported here were obtained using Eq. (7), this fact permits us to interpret these results in terms of just differences in the one-electron densities of states for the various structures. This has long been assumed in rigid-band approaches to phase stability, but now receives more rigorous justification through Eq. (9).

D. Comparison of GPT, LMTO, and AP methods

Beyond the local-density equations themselves, the principal approximations in the GPT method are (i) the small-core treatment (i.e., as atomiclike rather than bandlike) of the inner-core $2s$ and $2p$ levels, which is implicit in the construction of the pseudopotential w_0, and (ii) the neglect of higher-order terms in the electron density and total energy. Direct tests of the small-core approximation by LMTO calculations suggest that it is probably adequate up to at least fivefold compression in the third-period simple metals, and it is roughly up to this point that our GPT calculations have been carried out in each case. The all-electron LMTO method does not suffer this restriction, and in the present work LMTO phase-stability calculations have been done to tenfold compression.

Also with regard to the small-core approximation, the GPT core states, and hence the bare (unscreened) pseudopotential, are allowed to be properly volume dependent. That is, our small-core approximation is not a frozen-core approximation as is implicit in most other pseudopotential approaches including the AP method.[4] In the latter the bare-ion potential in the metal is replaced by a rigid bare pseudopotential constructed from the free atom. While this is a somewhat more restrictive pseudopotential approximation than is used in the GPT, tests have shown that it has negligible affect on the calculated structural energy differences in Si at least up to about twofold compression.[10]

With regard to phase stability the more significant approximation in the case of the GPT method is the neglect of higher-order structure-dependent terms. Intimately connected with this approximation is the choice of pseudopotential w_0 and d basis states ϕ_d. This choice is intended to be optimum in the sense of minimizing the importance of these terms. The available evidence both here and elsewhere suggests that this is indeed the case near normal conditions and under modest pressure. Beyond twofold compression, however, somewhat less localized d basis states may be required to achieve an equivalent quantitative description, at least in the case of Al, as will be discussed below. Both the LMTO and AP methods, on the other hand, are nonperturbative and thus implicitly retain the higher-order terms omitted in the GPT.

The principal approximation employed by the LMTO method is the atomic-sphere approximation, which has no counterpart in either the GPT or the AP method. According to this approximation, boundary conditions imposed at the Wigner-Seitz sphere surface are chosen to guarantee Bloch functions of the correct crystal symmetry; however, a spherical average of the resultant charge density is used in constructing the self-consistent one-electron potential as well as the total energy. Such an approximation should be best for the close-packed fcc and hcp structures where the correct Wigner-Seitz polyhedra are more nearly spherical, but less good for the more open-packed bcc structure with a less spherical Wigner-Seitz polyhedron. The atomic-sphere approximation should also be most effective in cases where shape-dependent electrostatic corrections [i.e., Eq. (8)] are relatively unimportant to the

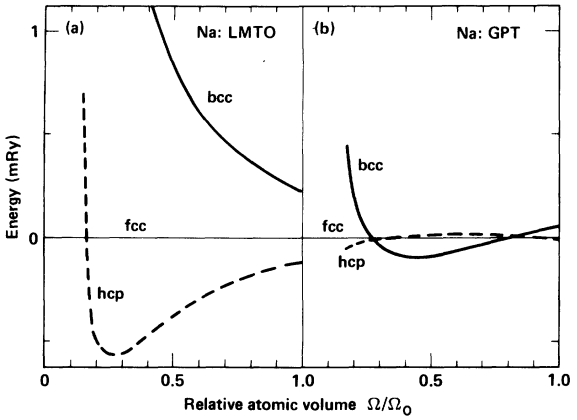

FIG. 1. Relative total energies of the bcc, hcp, and fcc structures of Na vs volume as calculated by the (a) LMTO and (b) GPT methods.

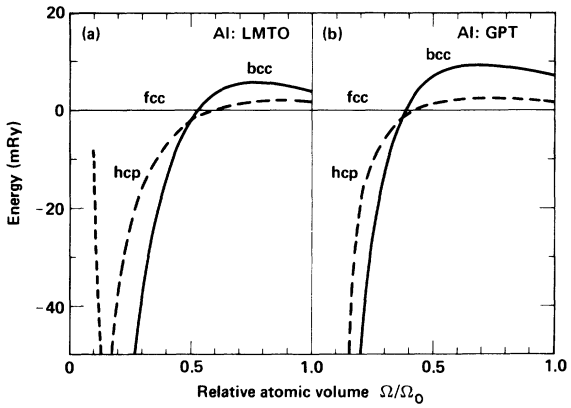

FIG. 3. Relative total energies of the bcc, hcp, and fcc structures of Al vs volume as calculated by the (a) LMTO and (b) GPT methods.

structural energy differences. In the present context, this is basically the case for Mg, Al, and Si, although not for Na.

With the exception of the pseudopotential approximation used in the AP method and possible concern about its continued accuracy under large compressions, the AP method appears to exactly solve the local-density equations. Both the GPT and LMTO methods make other approximations, as discussed, which leave them potentially less accurate in structural calculations than the AP method. Nevertheless, it should be noted that the comparative virtues of the GPT and LMTO techniques lie in vital areas. These include great computational speed, analytic separation of the tiny structural energy from the total energy in the GPT, and the ease with which the all-electron LMTO method can treat solids at any compression.

III. RESULTS

In this section we summarize our major predictions relating to phase stability in Na, Mg, Al, and Si. Our calculated zero-temperature structural energy differences for these materials are presented in Figs. 1–4, respectively. Each figure gives both (a) LMTO and (b) GPT results for the hcp and bcc total energies relative to that of the fcc phase as a function of reduced atomic volume Ω/Ω_0. Except for Si, Ω_0 is the experimentally observed 1-atm volume of each element. The stable 1-atm structure of Si is, of course, the semiconducting diamond phase ($\Omega_0=135$ a.u.). However, in order to stress the simple-metal behavior of this material at high pressure and to put Si on a comparable footing with Na, Mg, and Al, we have chosen the smaller volume $\Omega_0=97$ a.u. for Si. This value is the LMTO theoret-

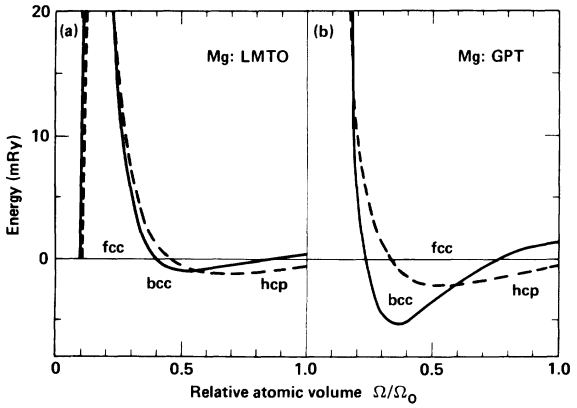

FIG. 2. Relative total energies of the bcc, hcp, and fcc structures of Mg vs volume as calculated by the (a) LMTO and (b) GPT methods.

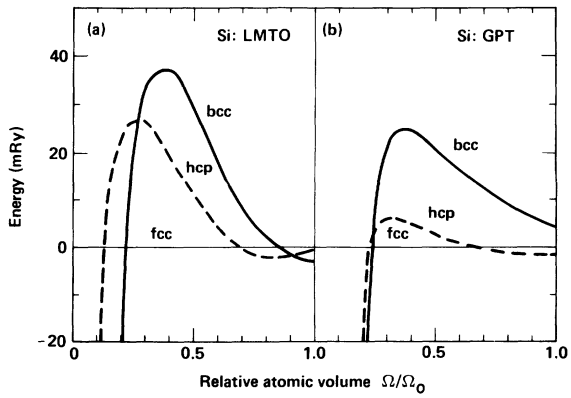

FIG. 4. Relative total energies of the bcc, hcp, and fcc structures of Si vs volume as calculated by the (a) LMTO and (b) GPT methods.

ical equilibrium atomic volume for the bcc structure. The corresponding zero-pressure volumes of the higher-energy fcc and hcp structures differ from this value by less than 3%.

There is excellent qualitative agreement between LMTO and GPT predictions for both the normal-density ($\Omega/\Omega_0=1.0$) stable structures in Na, Mg, and Al and the sequences of high-pressure structural phase transitions in Mg, Al, and Si, as indicated in Figs. 1–4. In the latter elements there is a one-to-one correspondence of all qualitative features obtained by the two methods throughout the region ($\Omega/\Omega_0>0.15$) where both methods have been employed. In this regard, the small region of bcc stability seen in the LMTO results for Si at the far right in Fig. 4(a) occurs in the GPT calculations beyond the volume range plotted in Fig. 4(b). Only for Na, where the structural energy differences are nearly 2 orders of magnitude smaller than those for Mg, Al, and Si, is there significant qualitative disagreement between LMTO and GPT predictions under compression, as can be seen in Fig. 1. This discrepancy will be discussed in Sec. V.

The GPT results given in Figs. 1–4 are those obtained from the empty-d-band limit of that theory. The importance of the d-state hybridization included in this limit increases with atomic number across the third-period elements and beyond twofold compression results in significantly improved agreement with our LMTO calculations in Al and Si as well as with the AP results of Lam and Cohen[20] in Al. This is shown directly for Al in Fig. 5 where both simple-metal and empty-d-band GPT energy differences are compared with the LMTO and AP results.

The predicted GPT and LMTO phase transitions implied by Figs. 1–4, as well as corresponding AP results in the cases of Al (Ref. 20) and Si (Ref. 5), are summarized in Table I. Also given in that table are the calculated transition volumes and pressures. The pressures listed are all LMTO-derived values at the stated volumes except for the AP Si pressures which are based on the work of Yin and Cohen.[5] In the case of the GPT-predicted hcp→bcc transition in Na, corrections for the zero-point vibrational energy have been included in Table I. The basic effect of the zero-point contribution is to lower the open-packed bcc energy relative to the close-packed fcc and hcp energies. This eliminates a tiny pocket of otherwise fcc stability in Na near $\Omega/\Omega_0=0.82$ and causes the bcc energy to drop below the hcp energy at $\Omega/\Omega_0=0.86$.

For completeness we have included in Table I the diamond→β-tin transition in Si as calculated by Yin and Cohen using the AP method.[5] This semiconductor-to-metal transition has been observed

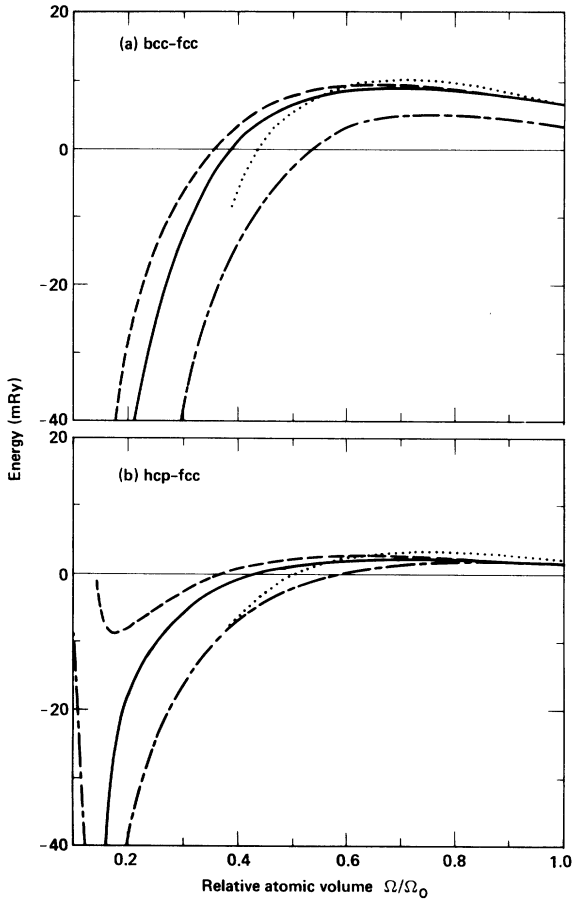

FIG. 5. Comparison of (a) bcc-fcc and (b) hcp-fcc total-energy differences for Al vs volume as calculated from the simple-metal and empty-d-band limits of the GPT (dashed and solid lines, respectively), the LMTO method (long-short dashed line), and the AP method (Ref. 20, dotted line).

experimentally at 12.5 GPa.[29] Our extrapolation of the Yin-Cohen results suggests a further β-tin→hcp transition at 41 GPa, by which point contact is made with the results in this paper. This β-tin →hcp transition bypasses the small region of apparent bcc stability at the right of Fig. 4(a). However, if Si should behave like another group-IV element, Sn,[30] a bct (body-centered-tetragonal) phase would have lower energy than this bcc structure, leading to the sequence β-tin→bct→hcp. In either case we are primarily concerned here with the simple-metal behavior of Si, which it seems reasonable to assume has become well established by the time Si has transformed into the hcp phase.

The mechanical stability of each of the predicted high-symmetry stable phases against distortion has also been tested by the GPT method, as described in Sec. II A. In all but one case the predicted stable

TABLE I. Predicted $T=0$ structural phase transitions in the third-period simple metals by the LMTO, GPT, and AP methods. Also compared are the atomic volume (Ω) and pressure (P) at the indicated transitions. Significant volume change across a transition is denoted by two values for Ω separated by a comma. Ω_0 is the observed 1-atm atomic volume except as noted.

Element	Ω_0 (a.u.)	Transition	Ω (a.u.) LMTO	GPT	AP	P (GPa) LMTO	GPT	AP
Na	255.2	hcp→bcc[a]		219			1	
		bcc→hcp[a]		71			104	
		hcp→fcc[b]	42			435		
Mg	156.8	hcp→bcc	88	91		57	50	
		bcc→fcc	63	37		180	790	
Al	112.0	fcc→hcp	65	48	54[c]	120	360	240[c]
		hcp→bcc	57	41	46[c]	200	560	420[c]
Si	135.1	diamond→β-tin			125,97[d]			10[d]
		β-tin→hcp			82,76[e]			41[e]
	97.0[f]	hcp→fcc	67	65		76	80	
		fcc→bcc	21	24		360	250	

[a]GPT predicted only.
[b]LMTO predicted only.
[c]Reference 20.
[d]Reference 5.
[e]Based on our extrapolations of the total-energy results of Ref. 5. Does not take into account the possibility of an intermediate bct structure (see, for example, Ref. 30).
[f]LMTO-predicted $P=0$ volume of the bcc phase, the most stable amongst the fcc, hcp, and bcc phases at this pressure.

phase was indeed found to be mechanically stable. The exception is the ideal hcp phase of Si for $\Omega/\Omega_0 > 0.67$. Our GPT calculations predict that the stable c/a axial ratio should be slightly higher than the ideal value of 1.633 in this volume range (e.g., $c/a = 1.67$ near the point of the possible β-tin →hcp transition), although this difference is not sufficiently large to compromise the hcp Si results reported here. In regard to the higher-energy structures, we also find mechanical instability for the bcc phases of Mg, Al, and Si for $\Omega/\Omega_0 > 0.88$, 0.55, and 0.34, respectively. This behavior is most pronounced in the case of Si and is consistent with the possibility of a lower-energy bct phase in this material at large volumes.

IV. ANALYSIS OF THE PHASE TRANSITIONS

The physical origin of the various structural trends predicted above for the third-period metals can be analyzed both in terms of the electronic band structure and in terms of the real-space pair potentials between atoms in the metal by the LMTO and GPT methods, respectively. We proceed with this analysis here before returning to discuss the quantitative significance of our results in Sec. V.

A. Relationship to electronic structure

Rather than discuss the phase transitions in each element individually, it is more illuminating to create a nearly equivalent generalized phase diagram appropriate to all. The LMTO force-relation technique offers the means of simply creating such a diagram if one varies both the number of valence electrons as well as the crystal structure, while using in all cases the same (e.g., fcc Al) set of self-consistent potentials. Figure 6 was obtained in this manner and illustrates regions of fcc, hcp, and bcc stability as a function of reduced atomic volume and number of valence electrons. Note that the sequences of phase transitions implied by Fig. 6, which has been obtained from model calculations *with the use of only the Al band structures,* are in complete qualitative agreement with the full LMTO predictions for compressed Na, Mg, Al, and Si seen in Figs. 1(a)–4(a), respectively.[31] The LMTO-predicted phase transitions in the third-period metals must therefore follow, at least qualitatively, simply from lattice-dependent differences in the one-electron band structure and the placement of the Fermi level (i.e., number of valence electrons). This is, of

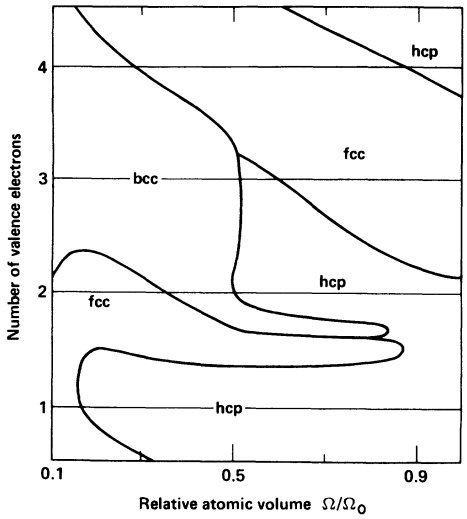

FIG. 6. Generalized phase diagram for the third-period simple metals as calculated from LMTO eigenvalue sums with the use of *only* the Al band structures. Stable phase is shown as a function of the number of valence electrons and atomic volume. Predicted transitions in this figure are in complete qualitative agreement with the full LMTO predictions in Figs. 1(a)–4(a).

course, the essence of a rigid-band model of phase stability.

Downward movement of the initially empty $3d$ band under compression plays a critical role in determining the high-pressure transitions seen in Fig. 6. To illustrate this movement, the fcc Al band structures at $\Omega/\Omega_0=1.0$ and 0.135 are shown in Figs. 7(a) and 7(b), respectively. Note in particular the two dotted-line segments, which are parts of the two lowest branches (X_1 and X_3, respectively) of the $3d$ band, and also one predominantly p-like region indicated by the dashed-line segment. At $\Omega/\Omega_0=1.0$ [Fig. 7(a)] the bands are basically free-electron-like, predominantly s and p in character (the sd-hybrid X_1 branch is mostly s-like here), and both dotted lines are seen to lie above the dashed line. Significant downward movement of the $3d$ band begins for compressions beyond about $\Omega/\Omega_0=0.5$, until by $\Omega/\Omega_0=0.135$ [Fig. 7(b)] it can be seen that both d-like dotted-line segments have moved below the p-like dashed-line segment. One consequence of this evolution, due in part to the symmetry-allowed interchange of the dashed and lower dotted segments in their connections with the rest of the band structure, is the appearance of a sharp dip in the fcc Al density of states at the intersection of the Q_1 and Q_2 branches in Fig. 7(b). As this point corresponds to two-electron occupation it is not surprising that our calculations show that fcc

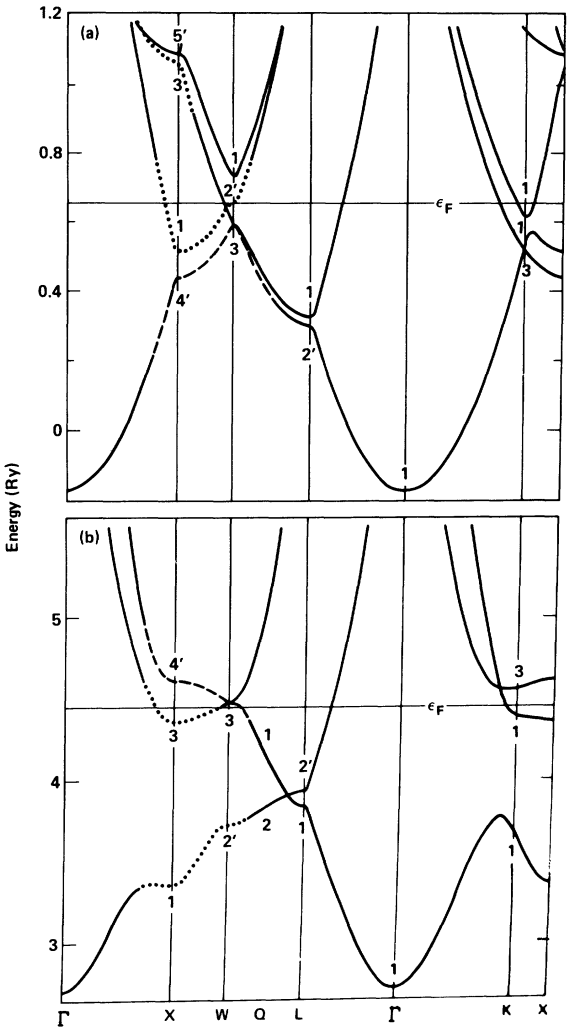

FIG. 7. LMTO band structure for fcc Al at (a) $\Omega/\Omega_0=1.0$ and (b) $\Omega/\Omega_0=0.135$. Dashed and dotted segments of the bands show particular regions of predominantly p and d character, respectively, as discussed in the text. Fermi level ϵ_F for Al is indicated.

Mg is a semimetal in the range $\Omega/\Omega_0=0.10$–0.15 for pressures from 2.4–6.2 TPa.[32] Such semimetal behavior is not uncommon for divalent fcc nearly-free-electron metals under compression.[16]

The increasing distortion of the band structure caused by the lowering of the $3d$ band appears, in fact, to be responsible for *all* of the high-pressure phase transitions predicted in Fig. 6 (and hence in the full LMTO results of Figs. 1–4). This has been demonstrated by performing LMTO calculations with the d character removed from the angular-momentum basis. We find in such calculations that Na, Mg, Al, and Si maintain hcp, hcp, fcc, and hcp stable structures, respectively, throughout the whole range $\Omega/\Omega_0=0.1$–1.0 shown in Fig. 6, i.e., there

would be *no* phase transitions in these simple metals in the absence of *d* electrons.[31]

Further insight into the structure in Fig. 6 is provided by examining the LMTO one-electron densities of states $\mathscr{D}(\epsilon)$ plotted in Figs. 8(a) and 8(b) for Al at $\Omega/\Omega_0=1.0$ and 0.135, respectively. Results for the fcc, hcp, and bcc phases are given, all obtained from self-consistent fcc Al potentials. Fermi energies ϵ_F for 1 through 4 electron occupation are marked at the top of the figures. Visual inspection

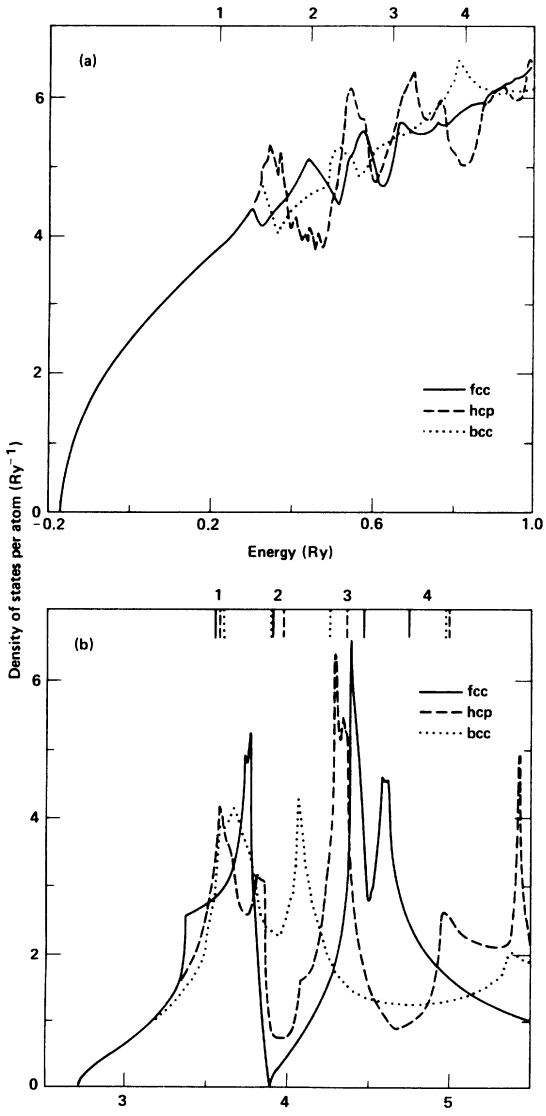

FIG. 8. LMTO density of states for Al at (a) $\Omega/\Omega_0=1.0$ and (b) $\Omega/\Omega_0=0.135$ for the fcc (solid lines), hcp (dashed lines), and bcc (dotted lines) structures. Fermi energies ϵ_F for 1 through 4 electron occupation are shown at the top of each plot. Only in (b) is there significant dependence of ϵ_F on structure.

of the $\mathscr{D}(\epsilon)$ is most instructive for the smaller of the two volumes although some insight is gained at the larger as well. For example, the free-electron character at larger volumes is easily seen in Fig. 8(a) at $\Omega/\Omega_0=1.0$ as the rough overall $\epsilon^{1/2}$ shape of the curves. The nearly-lattice-independent structure of these $\mathscr{D}(\epsilon)$ up to and slightly beyond one-electron occupation also shows why the structural energy differences for one-electron occupation (Na) are so small ($\sim$0.1 mRy) in comparison to those for Mg, Al, and Si. By two-electron occupation (Mg), however, the differences are O(1 mRy) and it can be seen why the hcp phase of Mg is favored at the larger volumes. Note the peak in the hcp $\mathscr{D}(\epsilon)$ near $\epsilon=0.35$ Ry in Fig. 8(a) and the dip near $\epsilon=0.45$ Ry. These features, in comparison to the $\mathscr{D}(\epsilon)$ for the other two phases, result in generally lower-energy hcp eigenvalues and give the hcp phase the lowest two-electron–occupation eigenvalue sum of the three lattices. However, this dip, combined with another hcp peak near $\epsilon=0.55$ Ry, works against the hcp phase when a third electron is added (Al).

Consider now the $\mathscr{D}(\epsilon)$ in Fig. 8(b) at $\Omega/\Omega_0=0.135$. The dramatic differences between these curves appear to simply explain the regions of pronounced fcc and bcc stability seen in Fig. 6 near and above two-electron occupation. The mathematical argument is the same as given above. Thus it is the fcc peak in the range $\epsilon\sim3.4$–3.8 Ry combined with the fcc semimetal dip near $\epsilon=3.9$ Ry which gives the fcc phase the lowest eigenvalue sum at two-electron occupation (Mg). Addition of a third valence electron (Al), however, finds both fcc and hcp phases with large peaks right at ϵ_F, leaving the bcc phase the most stable. Most of the large peaks in the $\mathscr{D}(\epsilon)$ are created by states near the bottom of the 3*d* band and their hybridization with the *sp* bands. The lowest-lying *d* states for the fcc structure occur in separate X_1 and X_3 branches, as discussed earlier, which are largely responsible for the buildup of fcc $\mathscr{D}(\epsilon)$ seen in Fig. 8(b) near the one- and three-electron Fermi levels, respectively. The dashed line in Fig. 8(b) shows a similar buildup of hcp $\mathscr{D}(\epsilon)$ to either side of the two-electron ϵ_F. In contrast to these close-packed structures, however, the bottom of the *d* band for the bcc structure occurs at only the single (although doubly-degenerate) H_{12} state. This may explain why large values of the bcc $\mathscr{D}(\epsilon)$ occur within a more narrow energy range ($\epsilon\sim3.5$–4.3 Ry) in Fig. 8(b) than is the case for the two close-packed structures. One consequence is that the three-electron ϵ_F falls at a low value of the bcc $\mathscr{D}(\epsilon)$, beyond the peak structure, causing this phase to be very stable relative to the fcc and hcp phases near three-electron occupation.

Skriver[16] has recently predicted analogous sequences of structural transitions at more modest compressions in Ca, Sr, Ba, and Ra due to the lowering of the $3d$, $4d$, $5d$, and $6d$ bands, respectively. He has shown that the structural energy differences for these alkaline-earth metals follow an almost universal curve as a function of the number of d electrons n_d. This behavior is consistent with our finding that the structural energy differences can be understood in terms of detailed features of the one-electron density of states. The same features should occur in the densities of states for all of the heavier alkaline-earth metals (beginning with Ca), provided the locations of the d bands relative to the sp bands are the same. It is precisely this information which the parameter n_d supplies. However, for the two light alkaline-earth metals Be and Mg there are no *nearby* d bands at normal density as there are for the heavier alkaline earths, and so one might expect the correlation with n_d to change. Indeed, we find the two transitions in Mg, hcp→bcc and then bcc→fcc, to occur for $n_d=0.23$ and 0.27, respectively. Neither this structural sequence nor the precise values of n_d closely correlate with Skriver's results for the heavy alkaline-earth metals, as is to be expected.

Lam and Cohen[20] have also analyzed the high-pressure Al transitions in terms of the number of d electrons. They note that the phase at $\Omega/\Omega_0=0.4$ which has the largest n_d will be stable because (i) the d component of the pseudopotential is more attractive than the s and p components in the core region, and (ii) the bcc phase will have the largest n_d because d orbitals overlap most strongly in this phase. While we believe this analysis to be essentially correct at $\Omega/\Omega_0=0.4$, we note that by $\Omega/\Omega_0=0.15$, where the bcc stability is most pronounced in our LMTO calculation, the bcc phase has the smallest n_d of the three phases. This indicates that determination of the stable phase in highly compressed third-period metals is not, in general, simply determined by the maximum n_d among the phases considered.

B. Relationship to interatomic potentials

We have used the characteristic functions Z^* and F_N directly in Eq. (2) for E_{struc} to obtain the GPT results presented in Sec. III above. In analyzing the physical meaning of these results, however, it is somewhat more revealing to work with the equivalent real-space representation of E_{struc}. Formally, E_{struc} can be written as a small structure-independent constant plus a lattice sum over a central-force pair potential between atoms. The resulting volume-dependent interatomic pair potential is given by

$$v_{\text{pair}}(r)=(Z^*e)^2\left[\frac{1}{r}-\frac{2}{\pi}\int_0^\infty F_N(q)\frac{\sin(qr)}{qr}dq\right]. \tag{10}$$

The first term in Eq. (10) is the direct Coulomb repulsion between ions of charge Z^*e, while the second term is the indirect ion-electron-ion attraction which screens the Coulomb interaction. At small separation r between atoms, less than the nearest-neighbor distance, the direct Coulomb interaction is dominant and a strongly repulsive pair potential results. At separations on the order of interatomic spacings, however, the repulsive and attractive contributions are comparable in magnitude and an oscillatory potential typically is obtained. At very large separations these become the familiar Friedel oscillations. These features are all clearly evident in the normal-density ($\Omega/\Omega_0=1.0$) interatomic potentials of Na, Mg, Al, and Si, which are plotted versus r/S in Figs. 9(a)–9(d), respectively.

In real space the clearest distinction in structural energies is between the open-packed bcc phase and the close-packed fcc and ideal hcp phases, largely because the latter phases have identical nearest and second-nearest neighbors. It turns out, in fact, that all of the GPT structural trends seen in Figs. 1(b)–4(b) for the bcc-fcc energy difference can be explained by considering only first-neighbor interactions in the fcc structure (12 total neighbors) and first- and second-neighbor interactions in the bcc structure (14 total neighbors). In this regard, note in Fig. 9 that $v_{\text{pair}}(r)$ for both Na and Mg has a distinct absolute minimum near the fcc nearest-neighbor distance. In Al this minimum is reduced to a shallow local one, while in Si only a strong inflection in the curve remains. Nonetheless, the existence of either a minimum or inflection at this point is sufficient in each case to make the bcc-fcc energy difference positive, in accord with the full GPT results of Figs. 1(b)–4(b). Under compression this minimum is slowly pressed out of the pair potential in a manner similar to the progression from Mg to Al to Si seen in Fig. 9, so that v_{pair} eventually becomes strongly repulsive at the first-neighbor distance. This is illustrated more clearly in the case of Mg in Fig. 10, where pair potentials at $\Omega/\Omega_0=1.0$ and 0.5 are compared. Whether or not the bcc-fcc energy difference remains positive under compression depends on the precise slope and curvature of this repulsive part of the potential. Under the right conditions, such as the very steep curve seen in Fig. 10 for $\Omega/\Omega_0=0.5$, the bcc-fcc energy difference becomes negative because the bcc second-neighbors are then unimportant and the energy difference is controlled by the fact that there are 12 fcc first neigh-

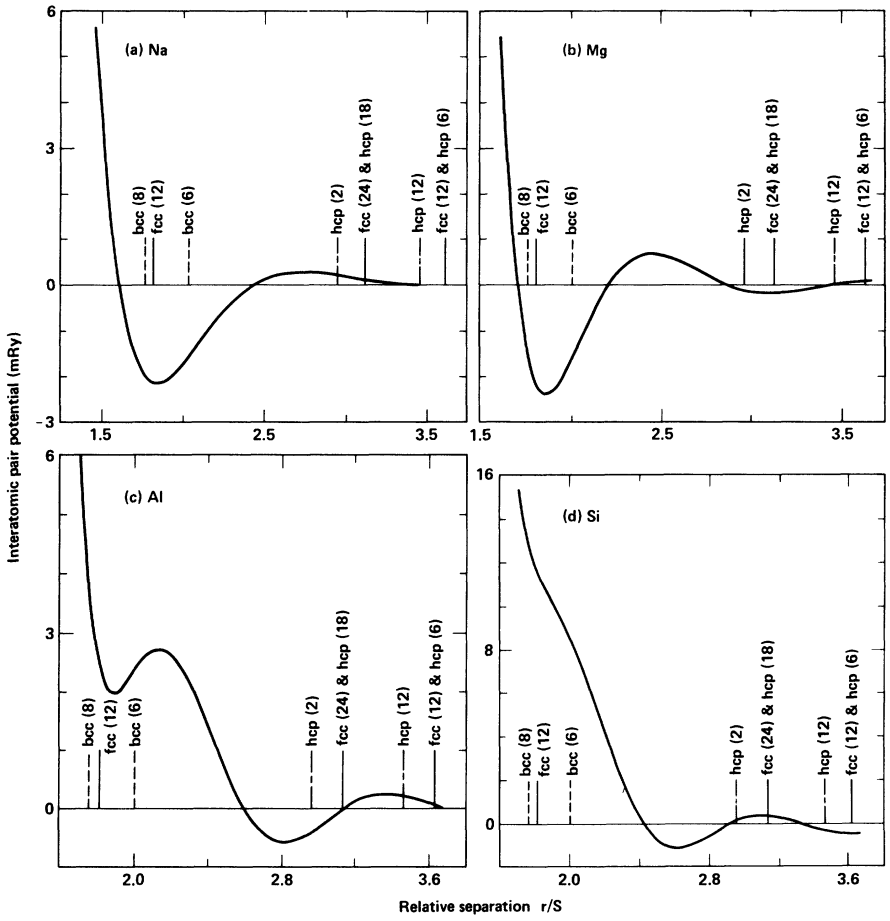

FIG. 9. Normal-density ($\Omega/\Omega_0=1.0$) interatomic pair potentials for (a) Na, (b) Mg, (c) Al, and (d) Si ($\Omega_0=97.0$) as calculated from the empty-*d*-band limit of the GPT. Location and number of the most structurally significant near neighbors for the fcc, hcp, and bcc lattices are indicated. [Note that the fcc and hcp structures have identical nearest and second-nearest (not shown) neighbors.] S is the Wigner-Seitz radius.

bors as opposed to only eight in the bcc structure. Suffice it to say that the correct trends are obtained in this manner in every case, as we have verified by direct calculation, although not accurately in the case of Na where the energy differences are so small.

A similar but necessarily more complicated analysis of the hcp-fcc energy difference is possible if one goes out to fourth-neighbor interactions in the fcc structure (54 total neighbors) and sixth-neighbor interactions in the ideal hcp structure (56 total neighbors). Visual study of Figs. 9(a)—9(d) implies, correctly, a negative hcp-fcc energy difference in Na and Si and a positive difference in Al, although, incorrectly, a positive difference in Mg also. However, extension of the analysis to smaller volume produces the correct trends [i.e., those seen in Figs. 1(b)—4(b)] in Mg, as well as in Al and Si, as we have directly verified. Only in Na does the analysis fail as a function of volume. This is undoubtedly an artifact of the incredibly tiny GPT hcp-fcc energy difference in that metal as seen in Fig. 1(b). In this regard, note from Fig. 9 that at a given reduced atomic volume the energy scale of interatomic potentials in all the third-period metals is roughly the same (1—10 mRy at normal density), so that the relative difficulty in analyzing Na in terms of v_{pair} becomes apparent.

V. QUANTITATIVE COMPARISONS

In this section we make a critical quantitative comparison of our GPT and LMTO results to each other, as well as to the recent AP calculations and to available experimental data. The existing experimental data on structural phase stability in the

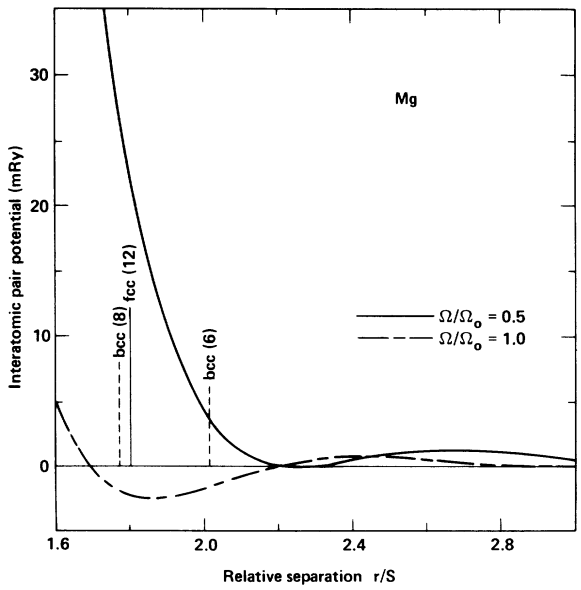

FIG. 10. Interatomic pair potential of Mg at both normal density ($\Omega/\Omega_0=1.0$) and twofold compression ($\Omega/\Omega_0=0.5$) as calculated from the empty-d-band limit of the GPT. Location and number of the fcc first neighbors and the bcc first and second neighbors are indicated. S is the Wigner-Seitz radius.

third-period metals is limited but is nonetheless useful in this comparison. In addition to the known stable structures at normal density there are experimental estimates of the energy differences between phases in Na, Mg, and Al. These data are given in Table II together with a summary of the corresponding $\Omega/\Omega_0=1.0$ GPT, LMTO, and AP predictions for these metals, as well as for Si.[33]

For Na the experimental bcc-fcc energy difference given in Table II has been obtained directly from the measured heat of transformation[34] in the well-known bcc→hcp Martensitic transition at about 36 K. Clearly, the GPT calculation of this number is in good agreement with the experimental value, while the corresponding LMTO result is more than a factor of 5 too large. Moreover, a GPT calculation[7] of the Martensitic transition temperature gives a quite reasonable value of 43 K. In Mg and Al, on the other hand, the experimental estimates are based on only extrapolations of thermochemical alloy data[36] and are of unknown reliability. This fact may be significant given the uniformly good agreement (to within 0.8 mRy) amongst the theoretical predictions for the hcp-fcc energy differences in Mg and Al, as compared to the less good (only to within

TABLE II. Structural energy differences ΔE_{tot} for the third-period simple metals as calculated from the LMTO, GPT, and AP methods. Results refer to the atomic volume Ω_0 shown, which is the observed 1-atm volume except for Si as noted.

Element	Ω_0 (a.u.)	Method	ΔE_{tot} (mRy) bcc-fcc	hcp-fcc	bcc-hcp
Na	255.2	LMTO	0.2	−0.1	0.3
		GPT	0.054	−0.011	0.065
		Expt.[a]			0.055
Mg	156.8	LMTO	0.2	−0.7	0.9
		GPT	1.4	−0.6	2.0
		Expt.[b]	2.0	−1.5	3.5
Al	112.0	LMTO	3.8	1.6	2.2
		GPT	7.3	1.7	5.6
		AP[c]	7.5	2.4	5.1
		Expt.[b]	7.7	4.2	3.5
Si	97.0[d]	LMTO	−3.0	−1.1	−1.9
		GPT	4.3	−1.6	5.9
		AP[e]	−3.1	−1.4	−1.7

[a]Measured heat of transformation (0.032, Ref. 34) less the calculated bcc-hcp difference in zero-point vibrational energies (−0.023, Ref. 35).
[b]Thermodynamically based estimates of Ref. 36.
[c]Reference 20.
[d]LMTO-predicted $P=0$ volume of the bcc phase, the most stable amongst the fcc, hcp, and bcc phases at this pressure.
[e]Reference 5.

about 2 mRy) agreement of these predictions with the experimental numbers in the table. At the same time in Mg and Al, the GPT and AP energy differences involving the bcc structure are in generally better agreement with each other and the experimental data than the LMTO values. We believe this latter situation is due to the less accurate treatment of more open-packed structures such as bcc by the atomic-sphere approximation in the LMTO method.

In the case of Si all of the calculated hcp-fcc energy differences in Table II are in close agreement (within 0.5 mRy), while the GPT and LMTO energy differences involving the bcc phase pull even farther apart following the trend established by the earlier elements. Both the numbers in Table II and the model calculations used in obtaining Fig. 6 show that the energy of the bcc structure relative to the close-packed structures increases with increasing valence until just beyond three-electron occupation. Further increase in the number of valence electrons reverses this trend, causing a rapid drop in the bcc energy, possibly related to an increased tendency towards covalency. Note that the AP method, which is best equipped to treat covalency, obtains the most dramatic decrease in the bcc-fcc and bcc-hcp energy differences from Al to Si. In the GPT results the corresponding decrease is much smaller, possibly due to the neglect of higher-order terms, leaving these two energy differences still positive for Si. In the case of the LMTO Si results, on the other hand, the close agreement with the AP calculations involving the bcc phase may be accidental in that the more modest drop in the LMTO bcc energy from Al to Si offsets the too low LMTO bcc energies already established for Mg and Al.

The validity of the GPT description of phase stability in Na is also supported by evidence at higher pressure. Above the Martensitic transition temperature, the bcc structure in Na is known to be quite stable under pressure. Resistivity data taken at 77 K indicates, in fact, that the bcc structure is stable up to at least 45 GPa.[37] This is entirely consistent with the GPT results in Fig. 1(b), but clearly not with the corresponding LMTO results in Fig. 1(a). The apparent failure of the LMTO method in Na is not just a matter of convergence uncertainties in the total energies, which are reliable to ~ 0.1 mRy, far too small to reconcile the GPT and LMTO results for this metal. Furthermore, the agreement between the two methods for the band structure and its volume dependence is as good if not better than that for the other three metals in the series. While electrostatic Ewald or Madelung contributions are quite important to an accurate description of Na, the major problem with the present LMTO calculations for this metal lies with the too large energy differences arising from the atomic-sphere approximation through Eq. (7). In comparison to this contribution, the omitted Ewald correction Eq. (8), is relatively unimportant. While the agreement between the LMTO and GPT predictions for Na is as good in an absolute sense (i.e., within 1 mRy) as that for any of the other three elements, it is clear that the structural energy differences in this material are simply too small to be obtained with even qualitative reliability within the atomic-sphere approximation of the LMTO method.

The available high-pressure experimental data for Mg, Al, and Si is generally less helpful. There has been some hint of an anomaly in room-temperature compressed Mg near 10 GPa, although whether or not this is due to a structural phase transition is not known.[38] There has also been the suggestion of a partial fcc$\rightarrow$hcp transition in Al at 20.5 GPa, though, as with Mg, these results are ambiguous.[39] In Si, however, the diamond—to—β-tin transition has been found experimentally at 12.5 GPa.[29] The 10-GPa AP prediction of Yin and Cohen[5] for this transition (Table I) is clearly in excellent agreement with experiment, lending support to the quantitative reliability of the AP method.

With regard to the GPT and LMTO methods, more revealing at high pressure in Mg, Al, and Si, is a direct comparison between the calculated energy differences themselves. Generally speaking, the quantitative distinction between the GPT and LMTO results increases as the metal is compressed. This is especially clear for Al, as can be seen from Fig. 5. Detailed analysis of this situation reveals that it is the respective treatment of the d states which is most responsible for this trend. In Fig. 11 the X_1 (sd-hybrid) and X_4' (p-like) fcc energy levels for Al are plotted relative to the Γ_1 level as a function of reduced volume. The dashed and solid lines indicate the simple and empty-d-band GPT results (negligibly different for X_4'-Γ_1), respectively, while the long-short dashed lines give the LMTO calculations. Note the excellent agreement between the GPT and LMTO values for the X_4'-Γ_1 separation, a rough measure of the width of the sp bands, at all volumes. In contrast there are significant differences between the methods for the X_1-Γ_1 separation at small volume. As the solid is compressed below $\Omega/\Omega_0=1.0$, the X_1-Γ_1 separation at first increases in response to the broadening sp bands. The lowering of the $3d$ band retards this behavior, eventually dominating near $\Omega/\Omega_0=0.25$, after which further compression decreases the X_1-Γ_1 separation. While the empty-d-band GPT result is in close agreement with LMTO at larger volumes, it deviates increasingly from the latter under compression, as if the d band were coming down more slowly than is the

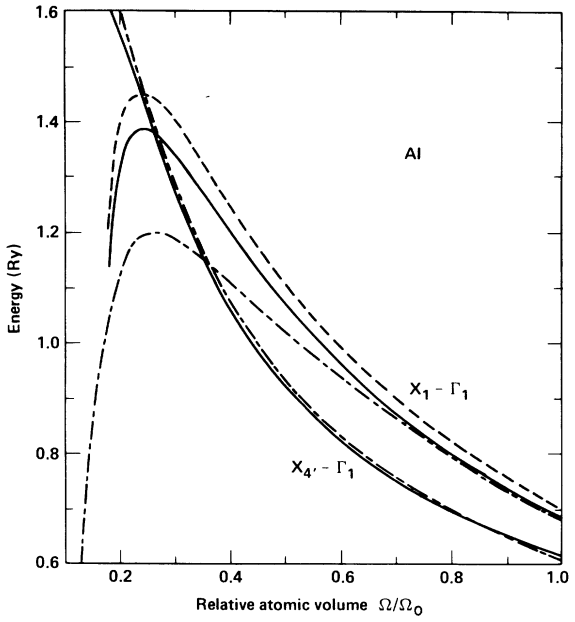

FIG. 11. Location of the $X_4'(p)$ and $X_1(sd)$ one-electron eigenvalues for Al relative to the bottom of the conduction band (Γ_1) vs volume as calculated from the simple-metal and empty-d-band limits of the GPT (dashed and solid lines, respectively) and from the LMTO method (long-short dashed line).

case in the LMTO calculations. This behavior is mirrored in the structural energy differences in Fig. 5. Because it is the lowering of the d band which drives the energy-difference curves downward with decreasing volume in Fig. 5, the GPT curves appear shifted to smaller volumes in relation to the LMTO results.

The LMTO method should be quite accurate in treating the relatively narrow $3d$ band and its hybridization with the sp valence states, as should the AP method as well. Thus it is significant that the AP results of Lam and Cohen[20] in Fig. 5, while in best agreement with the GPT calculations at large volumes, move into increasingly better agreement with the LMTO predictions at smaller volumes. This strongly implies that the empty-d-band GPT treatment of Al underestimates the d-state hybridization beyond about twofold compression, and that it is this fact which accounts for the growing quantitative differences between the LMTO and GPT results in this range. We have tested this more directly in Al at $\Omega/\Omega_0=0.40$ by arbitrarily lowering $E_d^{\rm vol}$ (and hence the $3d$ band) in the GPT equations. When $E_d^{\rm vol}$ is adjusted to reproduce the LMTO X_1-Γ_1 energy the bcc-fcc and hcp-fcc energy differences are indeed also reconciled. That is to say, under these conditions the GPT and LMTO energy differences agree as well at $\Omega/\Omega_0=0.40$ as they do at $\Omega/\Omega_0=1.0$. The same effect can be achieved more rigorously by choosing a less localized d basis state ϕ_d in the GPT theory. This suggests that while the prescription adopted for this choice is optimum in the vicinity of normal density, under high compression this is no longer true. In contrast, the excellent volume-independent agreement between the GPT and LMTO X_4'-Γ_1 energy, which is virtually independent of ϕ_d, shows that the pseudopotential w_0 does remain optimum even under high compression.

VI. CONCLUSIONS

We have demonstrated substantial qualitative and semiquantitative agreement between the predictions of the GPT and LMTO methods in regard to phase stability in the third-period simple metals, both near 1 atm and under high pressure. Only for the exceedingly small structural energy differences in Na is this agreement lacking, where the GPT method alone provides an adequate description of this material. With this exception, our GPT and LMTO results are not only in accord with each other, but are also in generally good agreement with the available experimental data and published AP calculations. Moreover, in the realm of possible diamond-anvil experiments, the GPT, LMTO, and AP results display sufficient quantitative consistency to be trusted as a guide to future experimental investigations. Clearly predicted here are the phase transitions (i) hcp→bcc in Na at ~1 GPa (~0 K only), (ii) hcp→bcc in Mg at ~50–57 GPa, and (iii) hcp→fcc in Si at ~76–80 GPa (following lower-pressure transitions to the hcp phase). At somewhat higher pressures we also predict an fcc→hcp transition in Al at ~120–360 GPa.

At least for Mg, Al, and Si, all of these transitions are driven by the downward movement of the $3d$ band under compression. While it is not possible as yet to translate this fact into simple comprehensive rules for phase stability in third-period simple metals, steps in this direction are provided by our analyses. For example, we have demonstrated that a rigid-band model of the electronic structure permits qualitative understanding of all of the LMTO-derived transitions. From a complementary point of view we have also shown how systematic trends in the interatomic pair potential, both with increasing atomic number at normal density and for individual elements under increasing pressure, are sufficient to

account for the GPT-derived transitions.

Finally, we have analyzed the quantitative accuracy of the GPT and LMTO methods as presently employed and have identified specific areas where either limitations occur or useful improvements could be made in structural energy calculations. These include the use of the atomic-sphere approximation in the LMTO method for open-packed lattices such as bcc and the choice of localized d basis states in the GPT at high compression.

ACKNOWLEDGMENTS

The authors wish to acknowledge a stimulating conversation with W. B. Holzapfel on structural phase stability in metals. One of us (A.K.M.) would also like to thank Dr. H. L. Skriver for his LMTO computer program. This work was performed under the auspices of the U. S. Department of Energy by Lawrence Livermore National Laboratory under Contract No. W-7405-Eng-48.

[1]A. Jayaraman, Rev. Mod. Phys. 55, 65 (1983).
[2]D. M. Adams and J. V. Martin, High Temp. High Pressures 13, 361 (1981).
[3]W. Kohn and L. J. Sham, Phys. Rev. 140, A1133 (1965).
[4]M. T. Yin and M. L. Cohen, Phys. Rev. B 25, 7403 (1982), and references therein.
[5]M. T. Yin and M. L. Cohen, Phys. Rev. Lett. 45, 1004 (1980); Phys. Rev. B 26, 5668 (1982).
[6]J. A. Moriarty, Phys. Rev. B 16, 2537 (1977).
[7]J. A. Moriarty, Phys. Rev. B 26, 1754 (1982).
[8]O. K. Andersen, Phys. Rev. B 12, 3060 (1975); O. K. Andersen and O. Jepsen, Physica (Utrecht) 91B, 317 (1977).
[9]A. R. Mackintosh and O. K. Andersen, in *Electrons at the Fermi Surface,* edited by M. Springford (Cambridge University Press, New York, 1980).
[10]A. K. McMahan, M. T. Yin, and M. L. Cohen, Phys. Rev. B 24, 7210 (1981).
[11]D. G. Pettifor, J. Phys. C 3, 367 (1970); N. W. Dalton and R. A. Deegan, *ibid.* 2, 2369 (1969); R. A. Deegan, *ibid.* 1, 763 (1968).
[12]B. Johansson and A. Rosengren, Phys. Rev. B 11, 2836 (1975).
[13]J. C. Duthie and D. G. Pettifor, Phys. Rev. Lett. 38, 564 (1977).
[14]Y. K. Vohra, H. Olijnik, W. Grosshans, and W. B. Holzapfel, Phys. Rev. Lett. 47, 1065 (1981). It has very recently been reported, however, that another group-III*B* element Sc shows a different sequence of transitions under compression. See Y. K. Vohra, W. Grosshans, and W. B. Holzapfel, Phys. Rev. B 25, 6019 (1982).
[15]J. A. Moriarty, Phys. Rev. B 8, 1338 (1973).
[16]H. L. Skriver, Phys. Rev. Lett. 49, 1768 (1982).
[17]The most recent and comprehensive experimental work on this sequence, however, indicates that the third structure for Ca and Sr is not hcp, although it has not yet been identified (W. B. Holzapfel, private communication).
[18]J. A. Moriarty and A. K. McMahan, Phys. Rev. Lett. 48, 809 (1982).
[19]C. Friedli and N. W. Ashcroft, Phys. Rev. B 12, 5552 (1975).
[20]P. K. Lam and M. L. Cohen, Phys. Rev. B (in press).
[21]L. Hedin and B. I. Lundqvist, J. Phys. C 4, 2064 (1971).
[22]U. von Barth and L. Hedin, J. Phys. C 5, 1629 (1972).
[23]The LMTO computer program used in this work is a modification of a program provided by H. L. Skriver [see, e.g., H. L. Skriver and J.-P. Jan, Phys. Rev. B 21, 1489 (1980)], and is described in A. K. McMahan, H. L. Skriver, and B. Johansson, *ibid.* 23, 5016 (1981).
[24]J. F. Janak, Phys. Rev. B 9, 3985 (1974).
[25]D. Glötzel and O. K. Andersen (unpublished).
[26]E. Esposito, A. E. Carlsson, D. D. Ling, H. Ehrenreich, and C. D. Gelatt, Jr., Philos. Mag. A 41, 251 (1980).
[27]D. G. Pettifor, Commun. Phys. 1, 141 (1976); D. A. Liberman, Phys. Rev. B 3, 2081 (1971).
[28]The force relation is discussed on pp. 187, 188, and 192 of Ref. 9. See also O. K. Andersen, H. L. Skriver, H. Nohl, and B. Johansson, Pure Appl. Chem. 52, 93 (1979), and V. Heine, in *Solid State Physics,* edited by H. Ehrenreich, F. Seitz, and D. Turnbull (Academic, New York, 1980), Vol. 35, pp. 114–120.
[29]J. C. Jamieson, Science 139, 762 (1963); 139, 845 (1963); B. A. Weinstein and G. J. Piermarini, Phys. Rev. B 12, 1172 (1975).
[30]J. Hafner, Phys. Rev. B 10, 4151 (1974).
[31]Owing to distortions in the volume scale inherent in the model calculations used to obtain Fig. 6, the bcc→hcp transition for Si seen at $\Omega/\Omega_0=0.92$ in Fig. 4(a) occurs beyond the range ($\Omega/\Omega_0>1$) plotted in Fig. 6. While this transition persists when d character is removed from the LMTO angular-momentum basis, it is probably not physically significant, as discussed in Sec. III.
[32]The lower pressure was erroneously cited as 24 TPa in A. K. McMahan and R. C. Albers, Phys. Rev. Lett. 49, 1198 (1982).
[33]The omitted Ewald correction Eq. (8) would change the LMTO results in Table II by less than about 25% in all cases. It causes the bcc-fcc and hcp-fcc differences to become more negative and more positive, respectively. The LMTO Al numbers in Table II are slightly different from those reported in Ref. 18 due to the use of improved sampling of the Brillouin zone.
[34]D. L. Martin, Proc. R. Soc. London Ser. A 254, 433 (1960).
[35]G. K. Straub and G. C. Wallace, Phys. Rev. B 3, 1234 (1971).
[36]L. Kaufman and H. Bernstein, *Computer Calculation of Phase Diagrams* (Academic, New York, 1970).
[37]R. Stager and H. G. Drickamer, Phys. Rev. 132, 124

(1963). See H. G. Drickamer, Rev. Sci. Instrum. 41, 1667 (1970), for the revised pressure scale.

[38]H. G. Drickamer, R. W. Lynch, R. L. Clendenen, and E. A. Perez-Alburene, in *Solid State Physics,* edited by H. Ehrenreich, F. Seitz, and D. Turnbull (Academic, New York, 1966), Vol. 19, p. 135.

[39]N. N. Roy and E. G. Steward, Nature (London) 224, 905 (1969).